university of groningen

University Medical Center Groningen

University of Groningen

Mg/Ti multilayers

Baldi, A.; Palsson, G. K.; Gonzalez-Silveira, M.; Schreuders, H.; Slaman, M.; Rector, J. H.; Krishnan, G.; Kooi, B. J.; Walker, G. S.; Fay, M. W.

Published in:
Physical Review. B: Condensed Matter and Materials Physics

DOI:
10.1103/PhysRevB.81.224203

IMPORTANT NOTE: You are advised to consult the publisher's version (publisher's PDF) if you wish to cite from it. Please check the document version below.

Document Version
Publisher's PDF, also known as Version of record

Publication date:
2010

Link to publication in University of Groningen/UMCG research database

Citation for published version (APA):
Baldi, A., Palsson, G. K., Gonzalez-Silveira, M., Schreuders, H., Slaman, M., Rector, J. H., Krishnan, G., Kooi, B. J., Walker, G. S., Fay, M. W., Hjorvarsson, B., Wijngaarden, R. J., Dam, B., Griessen, R., & Hjörvarsson, B. (2010). Mg/Ti multilayers: Structural and hydrogen absorption properties. *Physical Review. B: Condensed Matter and Materials Physics*, *81*(22), 224203-1-224203-10. [224203]. https://doi.org/10.1103/PhysRevB.81.224203

Copyright
Other than for strictly personal use, it is not permitted to download or to forward/distribute the text or part of it without the consent of the author(s) and/or copyright holder(s), unless the work is under an open content license (like Creative Commons).

The publication may also be distributed here under the terms of Article 25fa of the Dutch Copyright Act, indicated by the “Taverne” license. More information can be found on the University of Groningen website: https://www.rug.nl/library/open-access/self-archiving-pure/taverne-amendment.

Take-down policy
If you believe that this document breaches copyright please contact us providing details, and we will remove access to the work immediately and investigate your claim.

Downloaded from the University of Groningen/UMCG research database (Pure): http://www.rug.nl/research/portal. For technical reasons the number of authors shown on this cover page is limited to 10 maximum.

Download date: 05-05-2023

Mg/Ti multilayers: Structural and hydrogen absorption properties

A. Baldi,[1,2,*] G. K. Pálsson,[3] M. Gonzalez-Silveira,[1] H. Schreuders,[2] M. Slaman,[1,2] J. H. Rector,[1] G. Krishnan,[4] B. J. Kooi,[4] G. S. Walker,[5] M. W. Fay,[6] B. Hjörvarsson,[3] R. J. Wijngaarden,[1] B. Dam,[2] and R. Griessen[1]

[1]*Department of Physics and Astronomy, VU University Amsterdam, De Boelelaan 1081, 1081 HV Amsterdam, The Netherlands*

[2]*Department of Chemical Engineering, Delft University of Technology, Julianalaan 136, 2600 GA Delft, The Netherlands*

[3]*Department of Physics, Uppsala University, P.O. Box 530, S-751 21 Uppsala, Sweden*

[4]*Zernike Institute for Advanced Materials, University of Groningen, Nijenborgh 4, 9747 AG Groningen, The Netherlands*

[5]*Faculty of Engineering, University of Nottingham, University Park, Nottingham NG7 2RD, United Kingdom*

[6]*Nottingham Nanotechnology and Nanoscience Centre, University of Nottingham, Nottingham NG7 2RD, United Kingdom*

(Received 30 November 2009; revised manuscript received 6 April 2010; published 8 June 2010)

Mg-Ti alloys have uncommon optical and hydrogen absorbing properties, originating from a "spinodal-like" microstructure with a small degree of chemical short-range order in the atomic distribution. In the present study we artificially engineer short-range order by depositing Pd-capped Mg/Ti multilayers with different periodicities. Notwithstanding the large lattice mismatch between Mg and Ti, the as-deposited metallic multilayers show good structural coherence. On exposure to H_2 gas a two-step hydrogenation process occurs with the Ti layers forming the hydride before Mg. From *in situ* measurements of the bilayer thickness Λ at different hydrogen pressures, we observe large out-of-plane expansions of Mg and Ti layers on hydrogenation, indicating strong plastic deformations in the films and a consequent shortening of the coherence length. On unloading at room temperature in air, hydrogen atoms remain trapped in the Ti layers due to kinetic constraints. Such loading/unloading sequence can be explained in terms of the different thermodynamic properties of hydrogen in Mg and Ti, as shown by diffusion calculations on a model multilayered systems. Absorption isotherms measured by hydrogenography can be interpreted as a result of the elastic clamping arising from strongly bonded Mg/Pd and broken Mg/Ti interfaces.

DOI: 10.1103/PhysRevB.81.224203 PACS number(s): 68.65.Ac

I. INTRODUCTION

Magnesium and titanium are immiscible. Metastable Mg-Ti alloys have nevertheless been successfully prepared in thin films by high-energy processes, such as electron beam deposition[1] and magnetron sputtering.[2,3] These films have gravimetric hydrogen-storage capacities up to 6.5 wt % (Ref. 1) and fast and reversible kinetics of hydrogen absorption and desorption.[2] The structural reversibility of Mg-Ti alloys is particularly surprising when considering the strong segregation occurring in many Mg-based binary systems.[4,5] Furthermore, when exposed to H_2, Pd-capped Mg-Ti thin films switch from a reflecting metallic state to a black, light-absorbing, hydrogenated state.[2] This reversible optical black state can be applied in hydrogen sensors[6] and smart absorbers for solar collectors.[2,7] As also suggested by first-principles calculations,[8] the black appearance of the hydride is due to the formation of a face-centered-cubic phase, in which Mg and Ti atoms are distributed among the lattice sites with a certain degree of chemical short-range order,[9,10] leading to the coexistence of Mg-rich and Ti-rich regions with structurally coherent boundaries. Such "spinodal-like" microstructure is not uncommon in immiscible binary alloys[11,12] and it is a key ingredient in understanding the exceptional reversibility of Mg-Ti thin films.[10,13] In order to achieve a deeper understanding of the role of chemical segregation on the hydrogen-absorbing properties of these systems, we engineered one-dimensional short-range order by depositing several Mg/Ti multilayers with different periodicities. By controlling the degree of segregation of Mg and Ti we are capable of studying the influence of chemical order both on the structural coherence of our thin films and on their kinetics and thermodynamics of hydrogen absorption.

In the metallic state the multilayers are crystalline with partially coherent Mg/Ti interfaces. By means of structural studies we reconstruct their hydrogen-loading sequence, measure the out-of-plane expansion of the individual layers and detect the breaking of the structural coherence on hydrogenation. Such removal of coherence is responsible for the "scissor" effect observed in Ti-sandwiched Mg thin films:[14] when a thin Mg film is sandwiched between Ti layers it absorbs hydrogen at pressures close to bulk Mg, effectively behaving as quasifree. This is due to the fact that Mg and Ti, thanks to their positive enthalpy of mixing, form interfaces with poor adhesion, which become even more disconnected when Ti expands on hydrogen absorption. On the contrary, in Mg films capped with Pd, alloying occurs at the Mg/Pd interface and Mg feels an elastic constraint due to the presence of the cap layer that leads to higher equilibrium pressures of hydrogen absorption.[15] Mg/Ti multilayers prove to be an excellent playground to study a large number of physical phenomena, such as the influence of chemical segregation on the structural coherence of binary immiscible alloys, the impact of thermodynamics on the hydrogen-diffusion properties of layered media and the physical origin of clamping and surface energy effects in hydrogen-absorbing thin films.

II. EXPERIMENTAL DETAILS

Mg/Ti multilayers covered with Pd are deposited in a ultrahigh vacuum (UHV) compatible chamber (base pressure $=10^{-6}$ Pa) equipped with a computer controlled shutter sys-

 ©2010 The American Physical Society

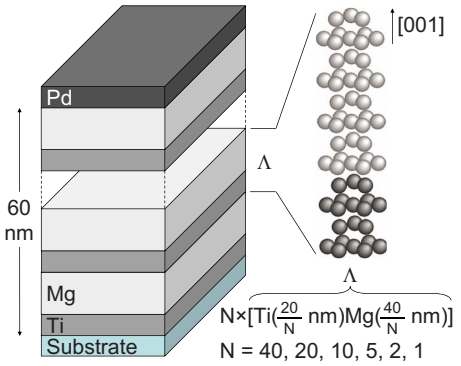

FIG. 1. (Color online) Sample geometry: the total multilayers thickness is 60 nm and, in every sample, Mg layers are twice as thick as Ti ones: $N\times[\mathrm{Ti}(\frac{20}{N}\ \mathrm{nm})\mathrm{Mg}(\frac{40}{N}\ \mathrm{nm})]$ with N=40, 20, 10, 5, 2, and 1.

tem, by dc and rf magnetron sputtering of Mg (99.95%), Ti (99.999%), and Pd (99.98%) targets in 0.3 Pa of Ar, on substrates kept at room temperature. The substrates used are $10\times10\times1$ mm^3 polished single-crystal Si(100) for x-ray diffraction (XRD), x-ray reflectivity (XRR), and high-resolution transmission electron microscopy (HRTEM), silicon nitride membranes for in-plane TEM and $10\times10\times0.5$ mm^3 float glass for hydrogenography measurements. In order to obtain homogenous films the substrates are continuously rotated during sputtering. The films are covered with Pd to prevent oxidation and promote hydrogen dissociation and absorption. The Pd thickness varies between 1 and 10 nm depending on the experimental technique used to analyze the samples. Typical deposition rates are 0.22 nm/s for Mg at 150 W (rf), 0.08 nm/s for Ti at 200 W (dc), and 0.11 nm/s for Pd at 50 W (dc). In each Mg/Ti sample the Mg layers are twice as thick as the Ti ones, giving, after correcting for the molar volumes ($\bar{V}_{\mathrm{Mg}}$=13.97 cm^3/mol, $\bar{V}_{\mathrm{Ti}}$=10.64 cm^3/mol), an overall composition of $\mathrm{Mg}_{0.60}\mathrm{Ti}_{0.40}$. The total multilayer thickness is 60 nm with six different bilayer thicknesses Λ, ranging from 1.5 to 60 nm: $N\times[\mathrm{Ti}(\frac{20}{N}\ \mathrm{nm})\mathrm{Mg}(\frac{40}{N}\ \mathrm{nm})]$ with N=40, 20, 10, 5, 2, and 1. These samples characteristics allow us to have fast and comparable kinetics of hydrogen absorption and desorption in all the multilayers. A sketch of the samples geometry is shown in Fig. 1.

XRD patterns are measured in a θ-2θ configuration, with a Bruker D8 Discover diffractometer equipped with a two-dimensional detector for real-time data collection over a large area with high sensitivity and low background. A beryllium dome allows *in situ* diffraction measurements during hydrogenation/deydrogenation of the films in hydrogen pressures up to 10^5 Pa and temperatures between room temperature and 473 K.

XRR measurements are performed on the 10× sample in a specially designed UHV chamber mounted on a Bruker Discover D8 x-ray diffractometer equipped with a parallel x-ray beam (Cu $K\alpha_1\lambda$=0.15406 nm), that allows *in situ* hydrogen loading in a wide range of temperatures and pressures.[16] The sample is measured at 333 K both in the as-deposited metallic state and during hydrogen uptake at different H_2 pressures. The temperature is high enough to promote fast kinetics of hydrogen absorption but low enough to avoid severe alloying at the Mg/Pd interface. In-plane resistance measurements are used to determine whether the dissolved hydrogen is in equilibrium with the surrounding H_2 atmosphere.

HRTEM was performed on a JEOL 2100F FEG-TEM, equipped with digital scanning transmission electron microscopy (STEM), Gatan Orius imaging system, and Gatan DigiScan. Cross-section samples were prepared by ion-beam milling using an FEI Quanta 200 ED FIB-SEM and transferred to the TEM using a Gatan HHST 4004 environmental cell and vacuum transfer holder to minimize oxidation.

Hydrogen-loading isotherms are measured at 333 K by means of hydrogenography,[17] an optical technique that allows to detect the amount of light transmitted through a thin film while slowly increasing the hydrogen pressure at constant temperature. The pressure-optical transmission-isotherms (PTIs) obtained by hydrogenography can be directly related to the standard pressure-composition-isotherms measured for metal hydrides.[18] Details of the hydrogenography experimental setup can be found in Gremaud *et al.*[17]

III. RESULTS AND DISCUSSION

A. Structural characterization: XRD, XRR, and TEM

1. As-deposited multilayers

The uncorrected XRD patterns measured for the as-deposited samples in vacuum at room temperature are shown in Fig. 2. Both Mg and Ti have hexagonal-closed-packed structures in their elemental form and the Mg/Ti multilayers grow with the (001) plane parallel to the substrate surface. For the 1× sample Ti and Mg layers are thick enough to give the reflections of pure elements, while already for the 5× sample superlattice peaks (satellite peaks) begin to appear, due to the repetitions of the bilayer thickness Λ. The broad peak appearing at ~40° for the 40× sample is the (111) reflection from the face-centered-cubic Pd. The absence of any Pd reflection in the patterns of the other multilayers is not surprising when considering that Pd is deposited on top of the uppermost Mg layer. Pd deposited on $\mathrm{Mg}_y\mathrm{Ti}_{1-y}$ thin films, in fact, does not produce any diffraction signal for $y>0.9$, although its presence is confirmed by Rutherford backscattering spectrometry.[13] Such peak disappearance is most likely due to the increase in lattice mismatch between Pd and $\mathrm{Mg}_y\mathrm{Ti}_{1-y}$ with increasing magnesium content, suggesting that for the 40× sample Ti and Mg layers are thin enough to undergo lattice deformations similar to the ones expected in a $\mathrm{Mg}_{0.6}\mathrm{Ti}_{0.4}$ alloy. In Fig. 2 we also show the simulated patterns obtained with an ideal step model, which assumes perfect superlattices with a square-wave composition modulation along the growth direction and coherent Mg/Ti interfaces.[19,20] In the simulations Ti and Mg interplanar distances, d_{Mg} and d_{Ti}, are fitted to take into account deviations induced by clamping from the substrate or quasiepitaxy in the multilayer and vary within ±1.4% with respect to their ideal values, Table I. The excellent agreement between nominal and fitted data indicates that the textured regions of our Mg/Ti multilayers correspond closely to their ideal geometries.

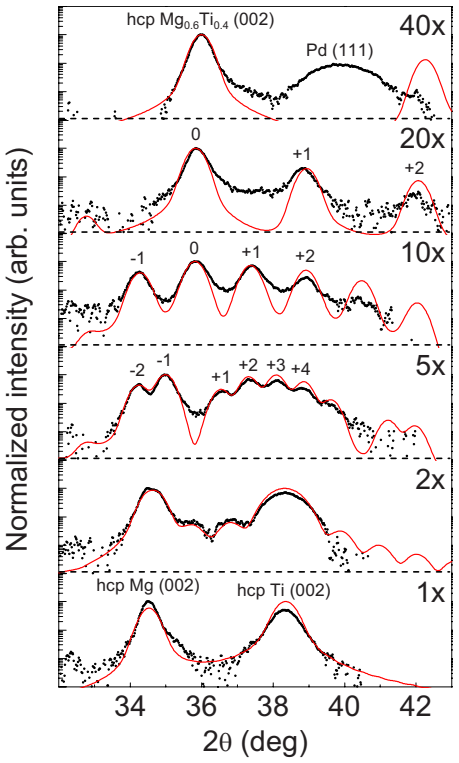

FIG. 2. (Color online) Measured (dots) and fitted (lines) XRD patterns of $N\times[\mathrm{Ti}(\frac{20}{N}\ \mathrm{nm})\mathrm{Mg}(\frac{40}{N}\ \mathrm{nm})]$ multilayers with $N=40$, 20, 10, 5, 2, and 1, covered with 5 nm of Pd. The simulations are based on idealized step model, not capturing the influence of defects and other imperfections.

In the model the diffracted intensity I is given by

$$I = I_{\mathrm{N}}(I_{\mathrm{Mg}} + I_{\mathrm{Ti}} + I_{\mathrm{MgTi}}), \tag{1}$$

where I_{N} is a term due to the N bilayer repetitions in the multilayers, I_{Mg} and I_{Ti} are the intensities of the constituent materials, and I_{MgTi} is a mixed term arising from the structural coherence.[20] In incoherent multilayers the mixed term disappears leading to a different distribution of intensities in the satellite peaks. The scattering powers of the elements are approximated with their atomic numbers and the patterns are filtered with a Gaussian distribution, with a full width at half maximum (FWHM) of 0.47°, to take into account the instrumental broadening and the possible deviations from a perfect geometry. These deviations include random variations in the number of atomic layers, differences in the microstructure at the interface with the substrate and with the Pd cap layer, distribution of sizes in in-plane grains and random orientations of the growth direction of each grain. Several models have been developed to include corrections to the ideal step model and take into account deviations from a perfect geometry.[19,21] In our XRD measurements, however, the experimental broadening is very high, on the order of 0.3°, due to the use of a two-dimensional detector that has a finite grid and requires a rather large beam spot on the sample in order to produce a high signal-to-noise ratio. Such a large experimental broadening hinders any attempt to obtain more detailed informations from the XRD patterns. Nevertheless, the simulations shown in Fig. 2 reproduce all the features observed experimentally, showing that on deposition Mg and Ti form well-defined layers with partially coherent interfaces. The structural coherence in Mg/Ti multilayers is rather surprising, given the 8.7% lattice mismatch between the in-plane cell parameter of Mg ($a_{\mathrm{hcp}}=0.3209$ nm) and Ti ($a_{\mathrm{hcp}}=0.2951$ nm). The rocking curve measured over the fundamental peak ($s=0$) of the 10× sample has a FWHM of 5.7°, indicating a moderately textured multilayer.

The 10× geometry, $10\times[\mathrm{Ti}(2\ \mathrm{nm})\mathrm{Mg}(4\ \mathrm{nm})]$, has been explored in more detail by means of *in situ* x-ray reflectivity at different hydrogen pressures. The XRR measurement of the as-deposited state of the multilayer, covered with 10 nm of Pd, is shown in Fig. 3(a): the measurement is conducted in vacuum (base pressure$=10^{-7}$ Pa) at 333 K. By fitting the XRD pattern measured at high angles on a sample deposited in the same run [inset in Fig. 3(a)] we obtain $\Lambda=5.66$ nm and $d_{\mathrm{Mg/Ti}}=0.2500$ nm. The XRR curve is simulated with GENX (Ref. 22) using the model in Fig. 1 to obtain the individual thicknesses of the constituent layers and the roughnesses at the interfaces. The software uses a dynamic optical model that incorporates effects arising from refraction, x-ray absorption, multiple scattering, instrumental resolution, and instrumental geometry. In the fit all the layer thicknesses and the interface roughnesses are varied. A layer of 1.7 nm of SiO_2 is added to the simulation on top of the Si (100) substrate to take into account the substrate surface oxidation. The results for the as-deposited state of sample 10× are summarized in the third column of Table II. The agreement between the Λ values obtained from the satellite peaks posi-

TABLE I. Comparison between nominal and fitted values for the bilayer thickness Λ, the interplanar distances d_{Mg} and d_{Ti}, and the average interplanar distance $d_{\mathrm{Mg/Ti}}$. All the values are given in nanometer.

	Nominal				Fitted			
	Λ	d_{Mg}	d_{Ti}	$d_{\mathrm{Mg/Ti}}$	Λ	d_{Mg}	d_{Ti}	$d_{\mathrm{Mg/Ti}}$
40×	1.5	0.2605	0.2343	0.2518	1.5	0.2580	0.2320	0.2493
20×	3.0	0.2605	0.2343	0.2518	3.0	0.2570	0.2372	0.2504
10×	6.0	0.2605	0.2343	0.2518	6.0	0.2585	0.2345	0.2505
5×	12.0	0.2605	0.2343	0.2518	12.0	0.2590	0.2359	0.2508
2×	30.0	0.2605	0.2343	0.2518	28.9	0.2590	0.2345	0.2509
1×	60.0	0.2605	0.2343	0.2518	59.9	0.2596	0.2345	0.2507

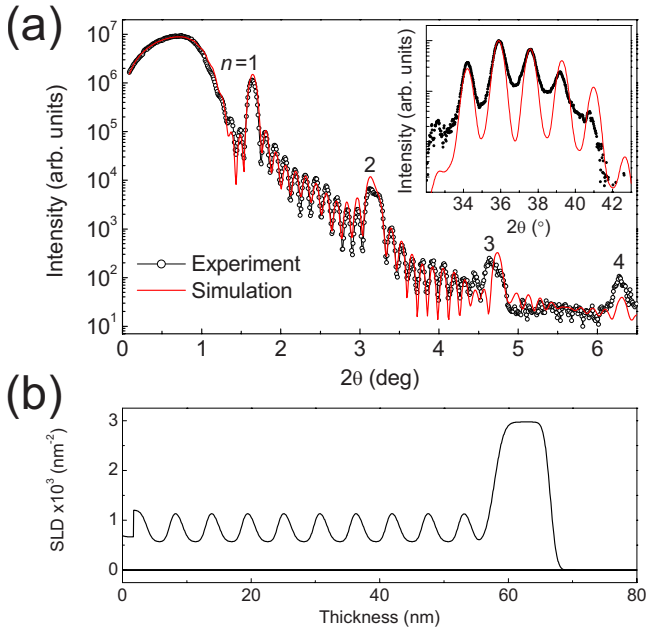

FIG. 3. (Color online) (a) X-ray reflectivity pattern of the 10× sample, 10×[Ti(2 nm)Mg(4 nm)]Pd(10 nm), taken at 333 K in vacuum (base pressure=10^{-7} Pa). The solid line is a simulation of the multilayer using GENX (Ref. 22). The inset shows the XRD pattern measured at high angles on a 10× sample deposited in the same run (dots) and the corresponding fit (line). (b) Real part of the SLD profile corresponding to the simulation in Fig. 3(a).

tion and from the simulation of the XRR pattern is excellent. The layers are flat with interface roughnesses on the order of one unit cell (assuming hcp Mg with c=0.521 nm and hcp Ti with c=0.469 nm). Figure 3(b) shows the real part of the scattering length density (SLD) profile corresponding to the simulation in Fig. 3(a). The SLD, which is given by the mass-density profile times the scattering lengths of the elements, gives an idea of the deviations from a perfect square-wave model that we have to introduce in the simulation, in order to accurately reproduce the experimental measurement.

TABLE II. Nominal and measured structural parameters of the 10× sample, 10×[Ti(2 nm)Mg(4 nm)]Pd(10 nm), as obtained from fitting the XRR patterns measured in vacuum (as deposited) and in 10^3 Pa of H_2 (fully hydrogenated): bilayer thickness Λ, layers thickness d, and roughness σ. All the values are given in nanometer.

	Nominal	XRR (vacuum)	XRR ($p_{H_2}=10^3$ Pa)
Λ	6	5.6	6.9
d_{SiO_2}		1.7	2.0
d_{Ti}	2	2.0	2.3
d_{Mg}	4	3.6	4.6
d_{Pd}	10	8.7	8.7
$\sigma_{Ti/Mg}$	0	0.74	1.0
$\sigma_{Mg/Ti}$	0	0.55	1.2
$\sigma_{Mg/Pd}$	0	1.2	1.3
$\sigma_{Pd/vacuum}$	0	0.78	1.1

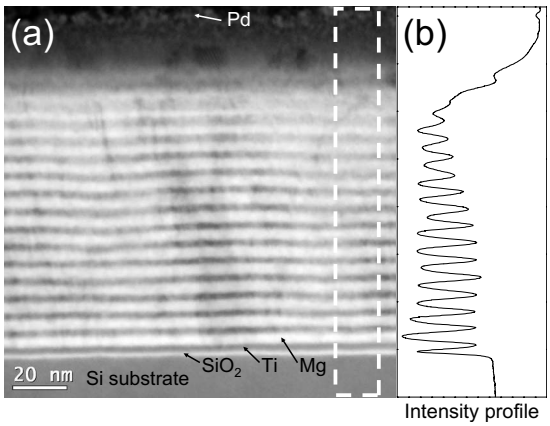

FIG. 4. (a) Cross-section bright-field STEM image of a 20×[Ti(2 nm)Mg(4 nm)] multilayer deposited on a Si(100) substrate and covered with 10 nm of Pd. (b) Intensity profile of the area delimited by a white dashed line.

In Fig. 4(a) we show the cross-section bright-field STEM image of a 20×[Ti(2 nm)Mg(4 nm)] multilayer, covered with 10 nm of Pd. The sample is well layered with slightly wavy Mg/Ti interfaces. Due to cumulative roughness, only 16 out of 20 bilayer repetitions are visible. Figure 4(b) shows the intensity profile of the area delimited by the white dashed line in Fig. 4(a). The maxima in the profile correspond to the bright Mg layers, except for the first (bottom) peak, which is attributed to the SiO_2 film covering the Si substrate. The effect of cumulative roughness is clearly visible in the intensity profile, where the peak-to-valley ratio decreases with increasing film thickness. Note that the sample measured in TEM is twice as thick as all the other investigated samples, in which the cumulative roughness effect is therefore going to be much smaller. Figure 5(a) shows a cross-section image of the same sample, in which it is clearly visible how the film is partially crystalline, with grains extending for several Mg/Ti repetitions, as already suggested by x-ray diffraction results. Figures 5(b) and 5(c) show a HRTEM image of the 20×[Ti(2 nm)Mg(4 nm)] multilayer and its Fourier transform, respectively. As expected, the multilayer has hexagonal closed-packed structure and grows along to the [001] direction. Although a slight decrease in crystallinity is observed with increasing thickness (not shown here), the crystal structure and orientation shown in Fig. 5(b) are visible across the multilayer from the substrate up to the Pd cap.

2. Hydrogen loading

When exposed to H_2 gas at room temperature, the Pd-capped Mg/Ti multilayers hydrogenate in two consecutive steps: (i) at lower H_2 pressures only the Ti layers form a hydride while Mg remains in its metallic state, (ii) at higher H_2 pressures also Mg absorbs hydrogen forming MgH_2. Such loading sequence is due to the lower (more negative) enthalpy of hydride formation of TiH_2[−65 kJ(mol H)$^{-1}$] (Ref. 23) with respect to MgH_2[−37.2 kJ(mol H)$^{-1}$] (Ref. 24) and can be detected both from XRD and XRR measurements.

Figure 6 shows the XRD patterns measured during loading and unloading of sample 10×. On loading the sample is

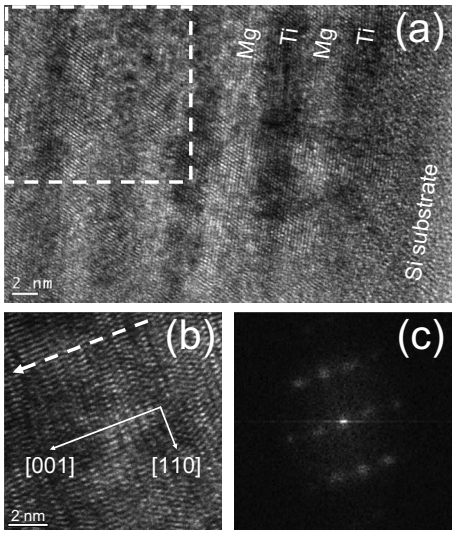

FIG. 5. (a) Cross-section TEM image of the 20× sample shown in Fig. 4. The dashed area highlights a region in which structural coherence is maintained across multiple Mg/Ti interfaces. (b) HR-TEM image of sample 20×, taken approximately in the middle of the multilayer. The dashed arrow, parallel to the [001] direction of the hcp structure, indicates the growth direction of the multilayer. (c) Fourier transform of Fig. 5(b).

exposed to 1 bar H_2 pressure at room temperature. The loading sequence shows an intermediate step in which only one peak is visible. This intermediate peak is similar to what is expected for a perfect hcp-(002) Mg/fcc-(111) TiH_2 multilayer, (circles in Fig. 6), although it is shifted to slightly lower angles, suggesting that Mg layers might also be partially hydrogenated. The final hydrogenated state shows poor crystallinity with a broad reflection at $2\theta \approx 34°$. When unloading the multilayer in air at room temperature the intermediate peak is recovered, suggesting that, due to kinetic limitations, hydrogen does not desorb from the Ti layers in the sample. A similar intermediate state, corresponding to a hcp-(002) Mg/fcc-(111) TiH_2 multilayer, is obtained for the

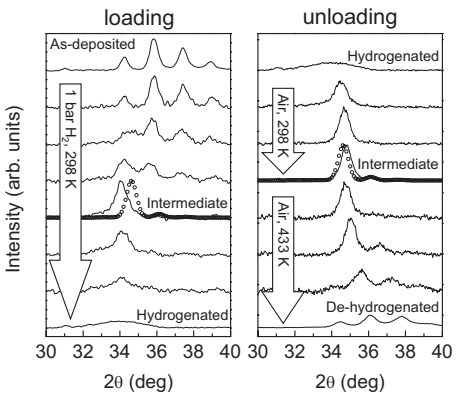

FIG. 6. XRD patterns measured during loading (left) and unloading (right) of the 10× sample, 10×[Ti(2 nm)Mg (4 nm)]Pd(10 nm). The intensities are normalized by the measuring times: 1 h for the "as deposited" and "hydrogenated" states, 5 min otherwise. Circles: simulations of a perfect hcp-(002) Mg/fcc-(111) TiH_2 10× multilayer.

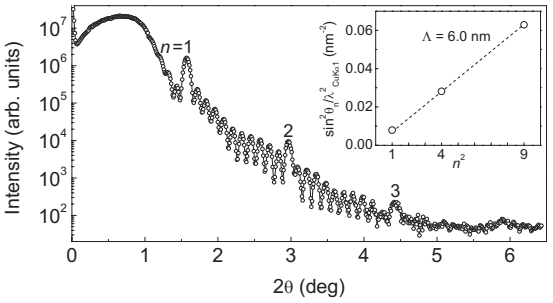

FIG. 7. XRR from the partially loaded 10× multilayer at $p_{H_2}=6$ Pa and $T=333$ K. The inset shows the measured linear dependence of the ratio $\sin^2\theta_n/\lambda^2_{\mathrm{Cu}\,K\alpha_1}$ versus n^2.

desorbed state of all the multilayers explored in the present work. In order to recover the initial metallic state the sample has to be heated in air at 433 K. Although the satellite peaks in the final dehydrogenated state are broader than in the as-deposited initial sample, it is remarkable that crystallinity appears again, after the large changes in volume on hydrogenation and dehydrogenation of Mg and Ti layers.

The intermediate state, characterized by the loading of the Ti layers only, has been explored in detail by measuring XRR on a 10× sample exposed to ~6 Pa of hydrogen at 333 K. Such a low pressure is enough to induce hydrogen absorption in Ti but not in Mg. This is confirmed by a decrease in the electrical resistivity of the multilayer on loading: unlike MgH_2, which is an insulator, TiH_2 is a metal with a higher electrical conductivity than Ti.[25]

Figure 7 shows the XRR pattern measured on the 10× sample at 333 K in ~6 Pa of hydrogen. From the position of the reflectivity peaks we can obtain the bilayer thickness Λ of such intermediate state according to[26]

$$\sin^2\theta_n = \left(\frac{\lambda_{\mathrm{Cu}\,K\alpha_1}}{2\Lambda}\right)^2 n^2 + 2\delta, \qquad (2)$$

where n is the order of the reflectivity peaks, as shown in Fig. 7, and δ is the deviation from unity of the real part of the average refractive index and, in first approximation, can be neglected.[16,21] From a linear fit of the plot $\sin^2\theta_n/\lambda^2_{\mathrm{Cu}\,K\alpha_1}$ versus n^2 (inset in Fig. 7) we calculate $\Lambda=6.0$ nm, corresponding to a period expansion of about 7% with respect to the as-deposited metallic state in which $\Lambda=5.6$ nm. According to the literature values for the molar volumes of Ti ($\bar{V}_{\mathrm{Ti}}=10.64$ cm^3/mol) and TiH_2 ($\bar{V}_{\mathrm{TiH_2}}=13.3$ cm^3/mol), the hydrogenation of titanium should expand the lattice of the host metal by 25%. Given the 3.6:2 thickness ratio of Mg and Ti measured by XRR (Table II) on the as-deposited sample, a uniaxial vertical expansion of the period Λ of 7%, due to the hydrogenation of Ti only, implies a vertical expansion of the Ti layers of about 20%. This can only be understood taking into account strong plastic deformations and out-of-plane material pile up, due to the hydrogen-induced in-plane coherency stress in the titanium layers.[27] This dramatic material movement is likely to remove the structural coherence at the Mg/Ti interfaces and to be at the origin of the "scissor" effect observed in Mg layers sandwiched between Ti thin films.[14,15]

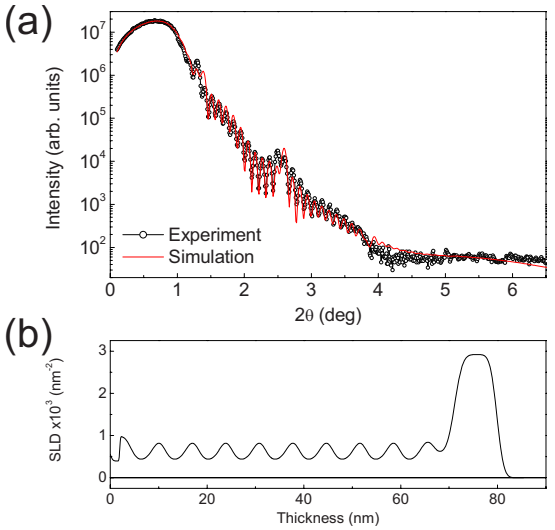

FIG. 8. (Color online) XRR pattern of the fully loaded 10× sample at $p_{H_2}=10^3$ Pa and $T=333$ K. The solid red line is a simulation of the multilayer using GENX (Ref. 22). (b) SLD profile corresponding to the simulation in Fig. 8(a).

After measuring the XRR of the intermediate state in ~6 Pa of H_2 at 333 K, we slowly increased the hydrogen pressure up to 10^3 Pa at constant temperature, following the hydrogenation of the film by measuring the changes in electrical resistance of the multilayer. After reaching equilibrium in 10^3 Pa of H_2 we measured the XRR pattern for the fully hydrogenated state, as shown in Fig. 8. The fit parameters used in the simulation in Fig. 8(a) are given in the fourth column of Table II. On hydrogenation the bilayer thickness Λ increases by 23%, from 5.6 nm in the as-deposited state to 6.9 nm in the fully hydrogenated state. Titanium layers expand by about 15%, from 2.0 to 2.3 nm, in good agreement with the value obtained from the period expansion observed on hydrogenation at 6 Pa (~20%). Magnesium layers expand by ~28% from 3.6 to 4.6 nm. In the hydrogenation of bulk Mg the molar volume increases by 30%, going from 13.97 cm^3/mol in Mg to 18.2 cm^3/mol in MgH_2: a uniaxial expansion of the Mg layers of 28% is therefore an indication of strong plastic deformations, due to the formation of defects and consequent out-of-plane pile up of MgH_2 grains.

The roughness increases observed on hydrogenation of the 10× multilayer could, in principle, be due to thickness variations or to interdiffusion of Mg and Ti atoms. In order to discriminate between these two phenomena we measured rocking curves across the second-order reflectivity peak, as shown in Fig. 9 for the as-deposited, intermediate, and fully hydrogenated sample. The pattern consists of two components, one narrow with a FWHM of 0.023° and one much broader. The narrow peak is the specular reflectivity and the width is what would be expected from an optically flat sample. The broader component comes from off-specular scattering which includes scattering from roughness at the interfaces. As can be seen in the figure, the off-specular contribution increases during loading, indicating an increase in interfacial roughness.[28,29] This is consistent with the reflectivity simulations which also showed a roughness increase on loading. This roughness increase could, in principle, also

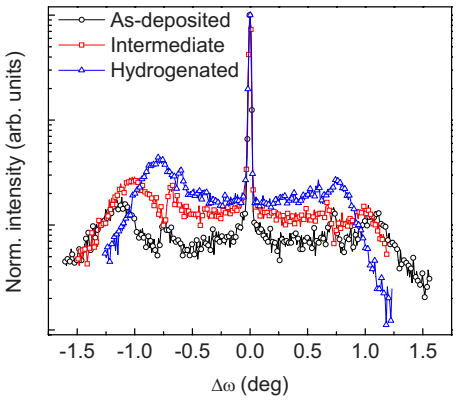

FIG. 9. (Color online) Rocking curves measured over the second-order reflectivity peak, for the as deposited, intermediate, and fully hydrogenated 10× sample. The scans are offset and only 50% of the experimental points are shown for clarity.

be attributed to atomic interdiffusion, however, since interdiffusion causes a lateral roughness with no particular length scale, it contributes zero or a constant amount to the off-specular scattering. The increase in the off-specular scattering observed in Fig. 9 is therefore due to an increase in roughness in the form of thickness variations. The small peaks at either side of the specular reflections are likely to be due to off-specular scattering from the first-order reflectivity peaks and not to correlations in the roughness.

Figure 10 shows the XRD patterns of the Mg/Ti multilayers measured after hydrogenation in 10^5 Pa at room tem-

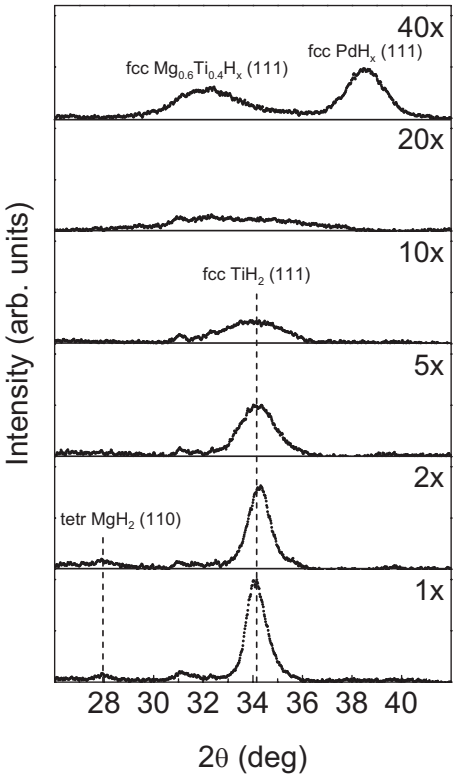

FIG. 10. XRD patterns measured for the 40×, 20×, 10×, 5×, 2×, and 1× multilayers after hydrogenation in 10^5 Pa at room temperature.

perature. The hydrogenated state of the 40× sample appears to be unique: it shows both the (111) reflection of fcc PdH_x (which is absent in the other samples, as already observed in the metallic state, see Fig. 2) and a peak analogous to the one measured for Ti-rich $Mg_yTi_{1-y}H_x$ alloys:[13] in codeposited Mg_yTi_{1-y} thin films, the hydrogenated state is tetragonal for $y>0.87$ and face-centered-cubic for $y<0.87$. Such fcc phase is similar to the one proposed for high pressure β-MgH_2 (Ref. 30) and originates from the structurally coherent dispersion of Mg-rich and Ti-rich nanosized domains in Mg-Ti thin-film alloys.[9,10] We therefore conclude that the 40× multilayer is structurally equivalent to a codeposited $Mg_{0.6}Ti_{0.4}$ alloy. The 20× sample shows a broad peak which suggests a microstructure intermediate between a fully layered and a mixed codeposited film. For the 10×, 5×, 2×, and 1× samples the (111) reflection of fcc TiH_2 is clearly visible. As expected the peak narrows with increasing Ti thickness in the multilayer. For 2× and 1× samples a small peak due to the (110) reflection of tetragonal (rutile) MgH_2 is also present. No traces of crystalline MgH_2 phases are, however, visible for 10× and 5× samples. In order to establish the crystal structure of MgH_2 in these samples we measured selected area electron diffraction (SAED) patterns of a hydrogenated 10× multilayer, covered with only 1 nm of Pd. Such small amount of Pd allows loading of the sample but its catalytic activity is rapidly suppressed by strong metal-support interaction effects[31] and it is not enough to promote significant hydrogen desorption.[13] The measurements were performed both for few seconds and for 10 min of electron-beam exposure. In the former case both tetragonal MgH_2 and face-centered-cubic TiH_2 peaks are observed, while in the latter hydrogen desorption from the MgH_2 layers occurs due to electron irradiation and reflections from hexagonal-closed-packed Mg are visible, Fig. 11. It is worth noting that in the hydrogenated state no signs of cubic MgH_2 are present. Apparently, the cubic hydride phase observed for codeposited Mg-Ti alloys can only be stabilized by a very fine three-dimensional dispersion of Mg and Ti atoms. A 10× multilayer, consisting of repetitions of 2 nm of Ti and 4 nm of Mg, is already too "segregated" and leads to standard tetragonal MgH_2. This result is consistent with the "scissor" effect observed in Ti-sandwiched Mg film, according to which no elastic interaction exists between adjacent Mg and Ti layers.[14]

B. Hydrogenography

In order to interpret the PTIs measured by hydrogenography on the Pd-capped Mg/Ti multilayers we make use of the following assumptions: (1) Mg layers in direct contact with Pd feel an elastic constraint, due to the formation of Mg-Pd alloys at the interface, which leads to plateau pressures higher than what expected from bulk Mg [$p^{333\ K}_{bulk\ Mg}=12$ Pa (Ref. 32)];[15] (2) in the process of Mg-Pd alloy formation typically 6 nm of Mg are "lost" and do not contribute to the optical change occurring on hydrogen absorption;[15] and (3) Mg films surrounded by Ti layers, on the contrary, do not feel significant elastic constraints, thanks to the positive enthalpy of mixing of Mg and Ti which leads to poor interface adhesion. Furthermore Ti absorbs hydrogen at lower pressures than Mg and the consequent lattice expansion removes the partial lattice coherence at the Ti/Mg interfaces and leads to quasifree Mg layers.[14] The PTIs measured at 333 K for the multilayers studied in the present work are shown in Fig. 12. The PTI for the 1× sample, Ti(20 nm)Mg(40 nm)Pd(10 nm), shows a relatively high plateau pressure with respect to bulk

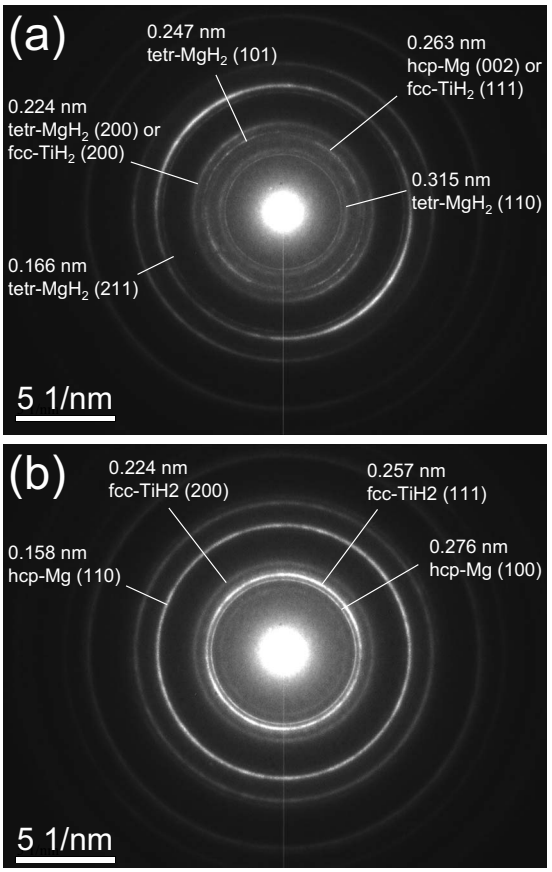

FIG. 11. SAED patterns for the hydrogenated state of a 10× Mg/Ti multilayer. (a) Short- and (b) long-beam exposures.

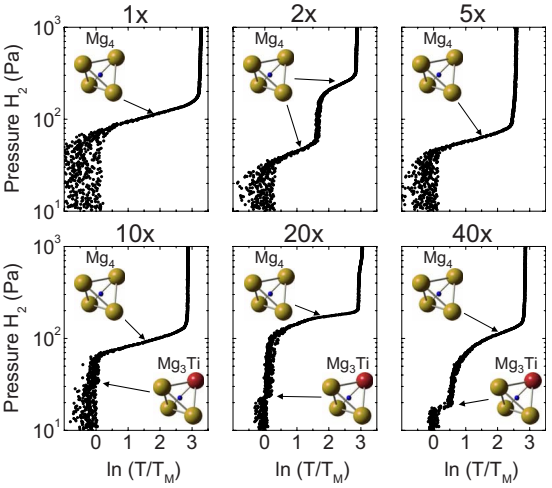

FIG. 12. (Color online) Loading pressure-transmission-isotherms measured by hydrogenography at 333 K for the Mg/Ti multilayers covered with 10 nm of Pd.

Mg ($p^{333\ K}_{bulk\ Mg}$=12 Pa),[32] due to the elastic clamping of the top Pd layer.[15] The same effect, together with the "scissor" property of Ti,[15] is responsible for the double plateau observed for the 2× sample, Ti(10 nm)Mg(20 nm)Ti (10 nm)Mg(20 nm)Pd(10 nm): the bottom Mg layer (lower plateau) is sandwiched between two Ti layers and it is therefore quasifree,[14] while the top one (higher plateau) is in contact with the Pd cover and feels its elastic constraint, therefore loading at higher hydrogen pressures. Following the same line of reasoning one would expect for the 5× sample to find two plateaus: a plateau at low pressure, build up by the bottom four Mg layers sandwiched between Ti and a plateau at higher pressure, coming from the top Mg layer in contact with Pd. The top plateau, however, is not visible due to the fact that the uppermost Mg layer is only 5 nm thick and therefore completely alloyed to Pd. In 10× and 20× the plateau pressure slightly increases with respect to the 5× sample. A possible explanation for such behavior is that in these two samples the individual Mg layers are very thin (4 nm, 2 nm, and 1 nm, respectively) and surface energy might provide a relevant contribution to the enthalpy of hydride formation.[33] For the 40× sample a sloping plateau similar to the one measured for a codeposited $Mg_{0.6}Ti_{0.4}$ alloy is observed,[17] suggesting that the microstructure of this sample is closer to a mixed alloy than to a well-defined multilayer.

It is worth noting that for 10×, 20×, and 40× samples a small plateau appears at very low hydrogen pressures. The width of this plateau is proportional to the number of Mg/Ti interfaces present in the multilayers. We interpret these plateaus as originating from hydrogen atoms populating the interstitial sites located at the Mg/Ti interfaces: in the metallic films the hydrogen atoms are located in interstitial tetrahedral sites, inside the Mg layers these are Mg_4 sites but, crossing the Mg/Ti interfaces, there will also be Mg_3Ti, Mg_2Ti_2, $MgTi_3$, and Ti_4 sites. Since the formation enthalpy of TiH_2 is smaller than the one of MgH_2, the substitution of one (or more) Mg atoms with Ti in a tetrahedral site will lower the absorption energy and the site will be populated at lower hydrogen pressures.[9]

C. Diffusion simulation of hydrogen cycling

While loading the multilayers in the XRD setup we exposed them to 1 bar of H_2 at room temperature, a pressure sufficient to hydrogenate both the Ti and the Mg layers. Nevertheless we observed an intermediate state in which only the Ti layers were loaded. Furthermore, on exposure to air at room temperature hydrogen desorbs from the Mg layers but remains trapped in the Ti ones and the original metallic state can only be recovered by heating the samples up to 433 K. These loading and unloading sequences can be qualitatively explained by looking at the difference in thermodynamic properties of hydrogen absorption in Mg and Ti. Pasturel *et al.*[34] have already shown how the chemical potential of hydrogen in different transition metals (*TM*) can influence the hydrogen-sorption kinetics in $Mg_2Ni/TM/Pd$ trilayers. Here we extend their model to a system with seven layers, in order to account for the multiple repetitions typical of a multilayer. The model treats hydrogen dissolved in metals in the lattice-gas approximation, without including any H-H interaction. The chemical potential of hydrogen in a metal (M) is therefore written as

$$\mu^M_H(c_M) = \bar{H}_H - T\bar{S}_H = \bar{H}_H - T(\bar{S}_{conf} + \bar{S}_{vibr}). \quad (3)$$

$\bar{H}_H$ and $\bar{S}_H$ are the partial molar enthalpy and entropy of hydrogen in metals, respectively. The configurational contribution to the entropy, $\bar{S}_{conf}$, is proportional to $\ln[c_M/(1-c_M)]$, where c_M is the hydrogen concentration in the metal. This term takes care that hydrogen atoms obey Fermi-Dirac statistics in the host metallic lattice, due to the single occupation of interstitial sites. In most metals the vibrational term, $\bar{S}_{vibr}$, is small at moderate temperatures and can be neglected with the significant exception of Pd [$\bar{S}_{vibr} \approx 19.2$ J K^{-1}(mol H)$^{-1}$ at 298 K].[35]

Each iteration of the model consists of two steps. First, the concentration within each layer is updated according to the diffusion equation. Subsequently, we impose the equality of chemical potential at the interface between two materials by changing the concentrations at the sites adjacent to the interface such that the chemical potential is made equal on both sites while keeping the *total* amount of hydrogen atoms unchanged. Note that the equality in chemical potentials at the interfaces does not imply the equality of hydrogen concentrations in the adjacent surfaces of the two layers. Instead of using the experimental values of the hydrogen pressure and the enthalpies and entropies of hydrogen absorption in Mg, Ti, and Pd we define the following dimensionless parameters:

$$e_H = \frac{1}{2}\ln\frac{p_{H_2}}{p^0},$$

$$e_M = \frac{\mu^M_H - \frac{1}{2}\mu^0_{H_2}}{RT} = \frac{\bar{H}_H - T\bar{S}_H - \frac{1}{2}H^0_{H_2} + \frac{1}{2}TS^0_{H_2}}{RT} = \frac{\Delta H_M}{RT} - \frac{\Delta S^0_M}{R}, \quad (4)$$

where $p^0=10^5$ Pa, ΔS^0_M is the entropy of hydride formation which, except for Pd [ΔS^0_{Pd}=−48.7 J K^{-1}(mol H)$^{-1}$], is taken equal to the entropy of hydrogen gas at standard pressure [$\Delta S^0_M \approx -\frac{1}{2}S^0_{H_2}$=−65 J K^{-1}(mol H)$^{-1}$], and ΔH_M is the enthalpy of hydride formation: ΔH_{Pd}=−20.5 kJ(mol H)$^{-1}$,[36] ΔH_{Mg}=−37.2 kJ(mol H)$^{-1}$,[24] and ΔH_{Ti}=−65 kJ (mol H)$^{-1}$.[23] Substituting these values in Eq. (4) and taking T=333 K, we obtain: e_{Pd}=−1.5, e_{Mg}=−5.6, and e_{Ti}=−15.6.

In Fig. 13, we simulate loading and unloading behaviors of a multilayer made of three Ti/Mg repetitions and covered with a Pd layer, in which the Mg layers are twice as thick as Pd and Ti ones: 3×[Ti(z)Mg($2z$)]Pd(z). In order to highlight

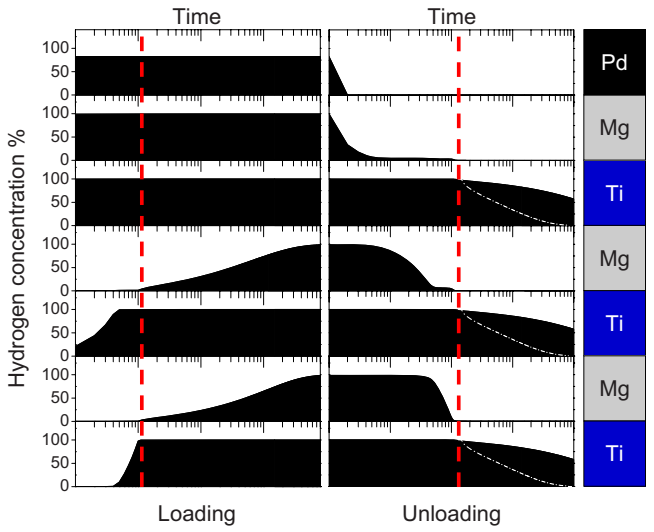

FIG. 13. (Color online) Simulated time evolution (in logarithmic scale) of the hydrogen concentration in each layer of a 3 $\times$[Ti(z)Mg($2z$)]Pd(z) sample, on hydrogen absorption (e_H=0) and desorption (e_H=−20). The vertical dashed lines represent the intermediate states, observed experimentally both on loading and unloading, in which only the Ti layers are hydrogenated. The white dashed-dotted lines are the simulated desorption rate from the Ti layers at 433 K.

only the effect of the chemical potential, we assume that the hydrogen-diffusion coefficient is the same for all the materials. The loading pressure is taken as 10^5 Pa(e_H=0) and the unloading pressure is taken negative enough in order to allow desorption from all the layers (e_H=−20). On exposure to 10^5 Pa of H_2, Pd and Ti layers and the uppermost Mg layer load very quickly, while the Mg layers "sandwiched" between Ti absorb hydrogen more slowly, effectively producing a transient intermediate TiH_2/Mg multilayer. This is due to the fact that at the beginning of the loading process, when the hydrogen concentration is low everywhere, Ti acts as a hydrogen sink due to its lower enthalpy of hydride formation, effectively sucking hydrogen atoms lying at the Ti/Mg interfaces. When the Ti layers are almost full the logarithmic entropic term in Eq. (3) dominates over the energetic term and Mg layers start to absorb hydrogen. On unloading the effect is opposite: at the beginning the hydrogen concentration is very high everywhere and hydrogen atoms remain trapped in the Ti layers until the adjacent Mg layers are "empty" enough to equilibrate the chemical potentials. When desorption starts in the Ti layers, however, the hydrogen concentration in the Mg layers is so low that the total flux of hydrogen atoms through Mg (which is proportional to the gradient in concentration) is minimal, resulting in a very slow hydrogen desorption. In Fig. 13 we also show that increasing the temperature of the system to 433 K enhances the rate of hydrogen desorption from the Ti layers (white dashed-dotted lines). With these simple simulations we can therefore give a qualitative interpretation of the persistence of hydrogen in the Ti layers, both on loading and unloading, as observed experimentally.

IV. CONCLUSIONS

We have prepared several Pd-capped Mg/Ti multilayers with various periodicities by means of magnetron sputtering. The deposited samples have lattice parameters in the z direction close to their nominal bulk values and low interfacial roughnesses. Partial structural coherence exists at the Mg/Ti interfaces in the as-deposited state but it is reduced on hydrogen absorption and desorption. The hydrogen loading sequence, as confirmed by both XRD and XRR, agrees with what is expected from thermodynamic considerations on the enthalpies of formation of magnesium and titanium hydrides: $Mg/Ti \rightarrow Mg/TiH_2 \rightarrow MgH_2/TiH_2$. Hydrogen absorption in both Ti and Mg layers leads to large expansions in the vertical out-of-plane direction, well beyond the elastic regime, indicating that massive material pile up, due to plastic deformations and creation of defects, has to take place. On unloading hydrogen is kinetically trapped in the Ti layers. Complete desorption only occurs on exposure to air at 433 K leading to the original metallic layered structure with a shorter coherence length. Magnesium hydride in a Mg/Ti multilayer with period Λ as small as 6 nm, retains its standard tetragonal structure, suggesting that the occurrence of a cubic hydrogenated phase, as observed in partially segregated Mg_yTi_{1-y}($y<0.87$) thin films,[9,10] can only be stabilized by a very fine dispersion of Mg-rich and Ti-rich domains. Pressure-optical transmission-isotherms measured by hydrogenography can be interpreted on the basis of the clamping effect on thin Mg films due to the adjacent layers[14,15] and, possibly, on the surface-energy differences between the metallic and hydrogenated states of ultrathin Mg films. A simple diffusion model allows us to reproduce both loading and unloading sequences measured experimentally.

ACKNOWLEDGMENTS

This work is financially supported by the Technologiestichting STW, the Nederlandse Organisatie voor Wetenschappelijk Onderzoek (NWO) through the Sustainable Hydrogen Programme of Advanced Chemical Technologies for Sustainability (ACTS) and the Marie Curie Actions through the Project No. COSY:RTN035366. One of the authors (B.H.) acknowledges support from Knut and Alice Wallenberg foundation. We thank S. De Man, V. Palmisano, and L. Mooij for fruitful discussion.

*Corresponding author; a.baldi@tudelft.nl

[1] R. A. H. Niessen and P. H. L. Notten, Electrochem. Solid-State Lett. **8**, A534 (2005).
[2] D. M. Borsa, A. Baldi, M. Pasturel, H. Schreuders, B. Dam, R. Griessen, P. Vermeulen, and P. H. L. Notten, Appl. Phys. Lett. **88**, 241910 (2006).
[3] S. Bao, K. Tajima, Y. Yamada, M. Okada, and K. Yoshimura, Sol. Energy Mater. Sol. Cells **92**, 224 (2008).
[4] I. A. M. E. Giebels, J. Isidorsson, and R. Griessen, Phys. Rev. B **69**, 205111 (2004).
[5] M. Gonzalez-Silveira, R. Gremaud, H. Schreuders, A. Baldi, B. Dam, and R. Griessen, Int. J. Hydrogen Energy (to be published).
[6] M. Slaman, B. Dam, M. Pasturel, D. Borsa, H. Schreuders, J. Rector, and R. Griessen, Sens. Actuators B **123**, 538 (2007).
[7] A. Baldi, D. Borsa, H. Schreuders, J. Rector, T. Atmakidis, M. Bakker, H. Zondag, W. van Helden, B. Dam, and R. Griessen, Int. J. Hydrogen Energy **33**, 3188 (2008).
[8] M. J. van Setten, S. Er, G. Brocks, R. A. de Groot, and G. A. de Wijs, Phys. Rev. B **79**, 125117 (2009).
[9] R. Gremaud, A. Baldi, M. Gonzalez-Silveira, B. Dam, and R. Griessen, Phys. Rev. B **77**, 144204 (2008).
[10] A. Baldi, R. Gremaud, D. M. Borsa, C. P. Baldé, A. M. J. van der Eerden, G. L. Kruijtzer, P. E. de Jongh, B. Dam, and R. Griessen, Int. J. Hydrogen Energy **34**, 1450 (2009).
[11] E. Ma, Prog. Mater. Sci. **50**, 413 (2005).
[12] J. H. He, H. W. Sheng, P. J. Schilling, C.-L. Chien, and E. Ma, Phys. Rev. Lett. **86**, 2826 (2001).
[13] D. M. Borsa, R. Gremaud, A. Baldi, H. Schreuders, J. H. Rector, B. Kooi, P. Vermeulen, P. H. L. Notten, B. Dam, and R. Griessen, Phys. Rev. B **75**, 205408 (2007).
[14] A. Baldi, V. Palmisano, M. Gonzalez-Silveira, Y. Pivak, M. Slaman, H. Schreuders, B. Dam, and R. Griessen, Appl. Phys. Lett. **95**, 071903 (2009).
[15] A. Baldi, M. Gonzalez-Silveira, V. Palmisano, B. Dam, and R. Griessen, Phys. Rev. Lett. **102**, 226102 (2009).
[16] G. K. Pálsson, A. R. Rennie, and B. Hjörvarsson, Phys. Rev. B **78**, 104118 (2008).
[17] R. Gremaud, C. Broedersz, D. M. Borsa, A. Borgschulte, P. Mauron, H. Schreuders, J. H. Rector, B. Dam, and R. Griessen, Adv. Mater. **19**, 2813 (2007).
[18] R. Gremaud, M. Slaman, H. Schreuders, B. Dam, and R. Griessen, Appl. Phys. Lett. **91**, 231916 (2007).
[19] B. Y. Jin and J. B. Ketterson, Adv. Phys. **38**, 189 (1989).
[20] C. Michaelsen, Philos. Mag. A **72**, 813 (1995).
[21] E. E. Fullerton, I. K. Schuller, H. Vanderstraeten, and Y. Bruynseraede, Phys. Rev. B **45**, 9292 (1992).
[22] M. Björck and G. Andersson, J. Appl. Crystallogr. **40**, 1174 (2007).
[23] *Phase Diagrams of Binary Hydrogen Alloys*, edited by F. D. Manchester (ASM International, Materials Park, OH, 2000), pp. 44073–0002.
[24] J. F. Stampfer, C. E. Holley, and J. F. Suttle, J. Am. Chem. Soc. **82**, 3504 (1960).
[25] M. Ito, D. Setoyama, J. Matsunaga, H. Muta, K. Kurosaki, M. Uno, and S. Yamanaka, J. Alloys Compd. **420**, 25 (2006).
[26] B. K. Agarwal, *X-Ray Spectroscopy: An Introduction* (Springer-Verlag, LLC, New York, 1991).
[27] U. Laudahn, A. Pundt, M. Bicker, U. v. Hülsen, U. Geyer, T. Wagner, and R. Kirchheim, J. Alloys Compd. **293-295**, 490 (1999).
[28] D. E. Savage, J. Kleiner, N. Schimke, Y.-H. Phang, T. Jankowski, J. Jacobs, R. Kariotis, and M. G. Lagally, J. Appl. Phys. **69**, 1411 (1991).
[29] H. Zabel, Appl. Phys. A: Mater. Sci. Process. **58**, 159 (1994).
[30] P. Vajeeston, P. Ravindran, A. Kjekshus, and H. Fjellvåg, Phys. Rev. Lett. **89**, 175506 (2002).
[31] A. Borgschulte, R. J. Westerwaal, J. H. Rector, B. Dam, R. Griessen, and J. Schoenes, Phys. Rev. B **70**, 155414 (2004).
[32] A. Krozer and B. Kasemo, J. Less-Common Met. **160**, 323 (1990).
[33] V. Berube, G. Chen, and M. S. Dresselhaus, Int. J. Hydrogen Energy **33**, 4122 (2008).
[34] M. Pasturel, R. J. Wijngaarden, W. Lohstroh, H. Schreuders, M. Slaman, B. Dam, and R. Griessen, Chem. Mater. **19**, 624 (2007).
[35] R. Gremaud, Ph.D. thesis, VU University Amsterdam, 2008.
[36] H. Frieske and E. Wicke, Ber. Bunsenges. Phys. Chem. **77**, 48 (1973).